

# Probing Structure–Nanoaggregation Relations of Polyaromatic Surfactants: A Molecular Dynamics Simulation and Dynamic Light Scattering Study

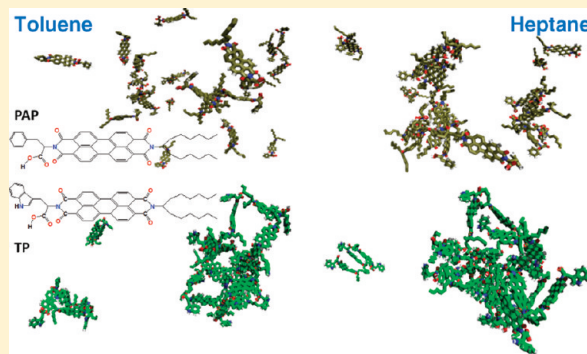
Robel B. Teklebrhan,<sup>†</sup> Lingling Ge,<sup>†</sup> Subir Bhattacharjee,<sup>\*,‡</sup> Zhenghe Xu,<sup>\*,†</sup> and Johan Sjöblom<sup>§</sup>

<sup>†</sup>Department of Chemical and Material Engineering and <sup>‡</sup>Department of Mechanical Engineering, University of Alberta, Edmonton, Alberta, Canada T6G 2G6

<sup>§</sup>Department of Chemical Engineering, Ugelstad Laboratory, Norwegian University of Science and Technology (NTNU), Trondheim NO 7491, Norway

## Supporting Information

**ABSTRACT:** Four synthetic perylene bisimide-based polyaromatic (PA) surfactants with a structural or functional group difference in their attached hydrophilic/hydrophobic substituent side chains were used to probe structure–nanoaggregation relations in organic media by molecular dynamics simulations and dynamic light scattering. The results from the simulated radial distribution functions and light scattering experiments indicate that variation in the structure of side chains and polarity of functional groups leads to significant variations in molecular association, dynamics of molecular nanoaggregation and structure of nanoaggregates. The aggregates of PA surfactant molecules grow to much larger sizes in heptane than in toluene. The aromatic solvent is shown to hinder molecular association by weakening  $\pi$ – $\pi$  stacking, demonstrating the control of molecular aggregation by tuning solvent properties. In aliphatic solvent, the aggregates formed from PA surfactants of aliphatic alkyl groups and phenylalanine derivatives as a side chain usually have a higher solvent accessible surface area to accessible volume ratio (SASA:AV) than that of tryptophan derivatives in their side chains. PA surfactants with an aliphatic functional group in both side chains does not form polyaromatic  $\pi$ – $\pi$  stacking (T-stacking) due to its strong steric hindrance in both solvents. Depending on the nature of the side chains attached, various stacking distributions, aggregation sizes, and SASA:AV ratios were obtained. In PA surfactant nanoaggregates, all of the solvent molecules were found to be excluded from the interstices of the stacked polyaromatic cores, regardless of whether the solvent molecules are aliphatic or aromatic. Although the change in the structure of side chain substituent in polyaromatic surfactants has a negligible impact on their self-diffusivity, it can strongly influence their intermolecular interactions, leading to different aggregate diffusion coefficients.



## 1. INTRODUCTION

“Structure dictates function” is a fundamental scientific tenet in materials, proteomics, biochemistry, and pharmaceuticals that utilizes structural information of macromolecules or nanoscale materials to understand its function.<sup>1–5</sup> What is common for this diverse multidisciplinary approach is to understand and detect the influence of molecular fingerprint on the first steps of molecular association into nanoaggregates, where these aggregates represent the first level of molecular clusters or building blocks in three-dimensional structures with immense importance in advanced three dimensional (3-D) materials, drug carriers, and so on.

In the past few years, constructing supramolecular nanomaterials from stacked polyaromatic building blocks has become a new phenomenon in the design of novel functional materials.<sup>6–9</sup> In polyaromatic stacking multiple  $\pi$ – $\pi$  interactions are involved.<sup>10,12</sup> To investigate  $\pi$ – $\pi$  stacking and the influence of different functional groups, individually or in

combination, on  $\pi$ – $\pi$  stacking and hence molecular assembly in organic media, perylene bisimide (PBI) with various attached hydrophilic/hydrophobic side chains has been used as a versatile polyaromatic building block. PBI is unique for its optoelectronic properties, thermal stability, multiple  $\pi$ – $\pi$  interactions, and high fluorescence quantum yields.<sup>13–16</sup> Perylene bisimide analogues have found widespread applications in many areas including organic thin film (or field-effect) transistors (OFETs),<sup>17</sup> organic (opto)electronic devices and sensors,<sup>18,19</sup> light harvesting arrays,<sup>20</sup> liquid crystals,<sup>21</sup> pigment and laser dyes,<sup>22,23</sup> and organic solar cells,<sup>24</sup> etc. Furthermore, polyaromatic-based functional arrays such as PBI analogues display a distinct electroactive and photoactive property due to their three-dimensional molecular assemblies.<sup>25,26</sup> The non-

**Received:** January 31, 2012

**Revised:** April 17, 2012

**Published:** April 18, 2012

Table 1. Compounds, Molecular Weights, and Structures of PA Surfactant Molecules<sup>a</sup>

Compound (Abbr.)	Mol. wt. (g/mol)	Molecular structure
<i>N,N'</i> - (1-hexylheptyl)-perylene-3,4,9,10-tetracarboxilic bisimide (BisA)	755 C <sub>50</sub> H <sub>64</sub> N <sub>2</sub> O <sub>4</sub>	
<i>N</i> -(1-hexylheptyl)- <i>N'</i> -(2-phenylpropanoic acid)-perylene-3,4,9,10-tetracarboxilic bisimide (PAP)	723 C <sub>46</sub> H <sub>46</sub> N <sub>2</sub> O <sub>6</sub>	
<i>N</i> -(1-hexylheptyl)- <i>N'</i> -(5-carboxylic pentyl)-perylene-3,4,9,10-tetracarboxilic bisimide (C5 Pe)	689 C <sub>47</sub> H <sub>48</sub> N <sub>2</sub> O <sub>6</sub>	
<i>N</i> -(1-hexylheptyl)- <i>N'</i> -(2-indol-3-yl-propanoic acid)-perylene-3,4,9,10-tetracarboxilic bisimide (TP)	762 C <sub>48</sub> H <sub>47</sub> N <sub>3</sub> O <sub>6</sub>	
<i>N</i> -(1-hexylheptyl)- <i>N'</i> -(methyl 2-phenylpropanoate)-perylene-3,4,9,10-tetracarboxilic bisimide (PCH)	721 C <sub>47</sub> H <sub>48</sub> N <sub>2</sub> O <sub>5</sub>	

<sup>a</sup>The synthesis and characterization of these PA surfactant molecules were reported elsewhere.<sup>38,46,47</sup> The molecular design of the PA surfactant molecules incorporates a polyaromatic perylene core with two alkyl chains attached to one end and a different functional group (polar or nonpolar) attached to the other end of the molecules.

covalent nature of the molecular association by polyaromatic stacking in turn brings about adaptivity and allows recycling of the functional materials.<sup>27</sup>

Although the construction of supramolecular nanostructures from polyaromatic building blocks in aqueous solutions are well-established,<sup>28–31</sup> little attention has been given to understanding the molecular association of polyaromatic building blocks in organic media despite its great importance in for example the petroleum industry.<sup>32,33</sup> It is well-known that polyaromatic associations in crude oil lead to precipitation and deposition of the condensed polyaromatic fraction of the crude oil during transportation and production, which results in blocking of reservoir rocks and transport pipes.<sup>34–37</sup> Furthermore, the polyaromatic association phenomena in crude oil strongly influence solubility, viscosity, density, and other physical properties of the crude oil.<sup>33–36</sup>

In this study, five well-defined polyaromatic surfactants (PA) based on perylene bisimide moieties were used as building blocks to probe the structure–nanoaggregation relationship in

organic media. All of these five molecules contain the same pronged aliphatic double chains on one side of the PBI. However, the other side of the PBI incorporates structural facets of different types of amino acids or aliphatic alkyl groups such as  $\beta$ -alanine, phenylalanine, tryptophan, and branched *n*-alkanes, making these molecules surface active.<sup>38</sup> Herein, we study the molecular association, nanoaggregate formation, and molecular dynamics of the polyaromatic surfactants in a bulk nonaqueous solution using molecular dynamics (MD) simulation and dynamic light scattering (DLS) measurement with the objective being to gain molecular insight into the hierarchy of interactions in molecular nanoaggregation.

## 2. SIMULATION METHOD

All of the classical MD simulations were carried out using the GROMACS 3.3.3<sup>39–41</sup> software package on a multiprocessor computing cluster (18 computer nodes: 4 cores at 2.2 GHz with 8 GB memory). The GROMOS96 force field<sup>42,43</sup> with the 53a6 parameter set was used in all calculations. This force field

is a united atom force field primarily parametrized for biological macromolecules, in particular for proteins and peptides, DNA, and phospholipids. The applicability of GROMOS96 force field to polyaromatic molecules<sup>44,45</sup> was first tested and shown to be useful and valuable in exploring the dynamics of polyaromatic nanoaggregate formation.

**2.1. Molecular Models.** Five PA surfactants shown in Table 1 are used in this study. These compounds are specially designed and synthesized in-house except for the last entry, *N*-(1-hexylheptyl)-*N'*-(methyl 2-phenylpropanoate)-perylene-3,4,9,10-tetracarboxylicbisimide (PCH). The PCH is a hypothetical compound and included in this study to investigate and probe the effect of a carboxylate group instead of a carboxylic acid group in polyaromatic surfactant on its nanoaggregation. PCH is a variation of *N*-(1-hexylheptyl)-*N'*-(2-phenylpropanoic acid)perylene-3,4,9,10-tetracarboxylicbisimide (PAP) in which the hydrogen atom of the hydroxyl group (-OH) is replaced by an alkyl group (-CH<sub>3</sub>). As compared with PAP molecules, this change of functionality from carboxylic acid (-COOH) to ester (-COOCH<sub>3</sub>) features a lower polarity of PCH molecules and weaker intermolecular hydrogen bonding. Including this compound in our study allows us to investigate the effect of the hydrogen bond network and polarity of the side chains on nanoaggregation of PA surfactants. The synthesis and characterization of the other four PA surfactants have been reported recently.<sup>38,46,47</sup>

The initial molecular geometries (PDB coordinates) of these PA surfactant molecules were obtained using Chem 3D ultra 10.0 software.<sup>48</sup> The coordinates of these PA surfactant molecules were then transferred, as an input file, to the PRODRG 2.5<sup>49</sup> server to generate the necessary molecular topology and GROMACS structure files. All of the double bonds and aromatic rings were modeled with sp<sup>2</sup> hybridized carbons. Furthermore, the polar and aromatic hydrogen atoms were modeled explicitly while aliphatic hydrogens were treated as unified interaction sites (hence, united-atom models). In our simulations, toluene and heptane were used as solvents of two extreme polarities or solvent qualities. The topology of toluene was generated from phenylalanine amino acid fraction through the *pb2gmx* routine in GROMACS. Lipid aliphatic chain was used for heptane. Heptane is a nonpolar molecule; its atomic charge was therefore set to zero for all interaction sites. The topologies of the PA surfactant molecules and the organic solvents are available upon request.

**2.2. Simulation Setup and Conditions.** Molecular dynamics simulation of five well-defined PA surfactant molecules in toluene and heptane was performed over the time range of 20 ns. Initially, the dimensions of the simulation boxes were set at 12 nm × 12 nm × 12 nm. A total of 10 simulation boxes were constructed with each box containing 24 molecules of a single type of PA surfactant molecules in an ordered and random placement.

The systems were solvated with either toluene or heptane molecules. After setting up the initial configurations, the system energy was minimized using the steepest descent and conjugate gradient methods as implemented in GROMACS 3.3.<sup>39–41</sup> A cutoff of 1.2 nm was used for both Coulomb and van der Waals interactions during energy minimization. The hydrogen-bond interaction is considered as a form of electrostatic interactions in molecular modeling.

The system maximum force was converged to less than 200 kJ mol<sup>-1</sup> nm<sup>-1</sup> threshold set to generate a stable system for the simulations. The detailed information on the simulated systems

is listed in Table 2. All simulations were carried out under the NPT ensemble at 298 K and 1 bar pressure. For the first 3 ns, the Berendsen thermostat and barostat<sup>50</sup> were used to quickly relax the system to a constant pressure and temperature. After 3 ns, all of the simulations were performed using Nosé–Hoover thermostat<sup>51,52</sup> and Parrinello–Rahman pressure coupling algorithm.<sup>53</sup> The pressure and temperature coupling constants of  $\tau_p = 3$  ps and  $\tau_T = 0.3$  ps, respectively, were used throughout the simulations. In all simulations, an isothermal compressibility of  $1.47 \times 10^{-4}$  bar<sup>-1</sup> and  $9.08 \times 10^{-5}$  bar<sup>-1</sup> were applied for heptane and toluene, respectively.<sup>54</sup>

Periodic boundary condition (PBC)<sup>55</sup> was applied in the *x*, *y*, and *z* directions, and a leapfrog Verlet algorithm<sup>56,57</sup> with a time step of 2 fs was used for integration of the trajectories. The electrostatic interaction was computed using the particle-mesh Ewald summation (PME)<sup>58</sup> method with a fast Fourier transform (FFT) grid spacing of 0.16 nm to account for long-range electrostatic interactions of the system. A cutoff of 1.4 nm was used for the van der Waals interactions and is consistent with GROMOS96 parametrization.

All bond lengths in our system were constrained using LINCS algorithm.<sup>59</sup> A neighbor list with a cutoff of 1.2 nm was updated every 5 steps. The initial atomic velocities of the system were set using the Maxwell–Boltzmann distribution employed in GROMACS at the specified temperature of 298 K. After simulations for 20 ns, the structure and dynamic properties of the system were analyzed using the GROMACS built-in analytical tools. The time evolutions of the structure of the system were also visualized using visual molecular dynamics (VMD).<sup>60</sup>

### 3. EXPERIMENTAL METHODS

**3.1. Materials and Solution Preparation.** Synthesis and structural characterization of the PA surfactant molecules were performed at the Ugelstad Laboratory (NTNU, Trondheim, Norway). The PA surfactant molecules passed an extra purification step with flash chromatography as described elsewhere.<sup>38,46,47</sup> Pertinent information regarding these compounds is provided in Table 1. The compounds were dissolved in toluene (Fisher Scientific, optima grade) under sonication. For dynamic light scattering experiments, the solutions prepared were filtered through 0.45 μm PTFE filters (Millipore) directly into dust-free light scattering cells, which

Table 2. Composition of Simulation Systems

system	PA surfactant molecules	time (ns)	<i>N</i> <sub>solvent</sub>	final volume size (nm <sup>3</sup> )
Simulation A: 24 PA Surfactant Molecules in Toluene				
BT3	BisA	20	5571	9.96 × 9.96 × 9.96
PT1	PAP	20	5601	9.99 × 9.99 × 9.99
CT2	CS Pe	20	5601	9.98 × 9.98 × 9.98
TT4	TP	20	5591	9.97 × 9.97 × 9.97
PT5	PCH	20	5598	9.97 × 9.97 × 9.97
Simulation B: 24 PA Surfactant Molecules in Heptane				
BH8	BisA	20	4660	10.44 × 10.44 × 10.44 <sup>a</sup>
PH6	PAP	20	3898	9.89 × 9.89 × 9.89
CH7	CS Pe	20	3911	9.86 × 9.86 × 9.86
TH9	TP	20	3905	9.87 × 9.87 × 9.87
PH10	PCH	20	3907	9.90 × 9.90 × 9.90

<sup>a</sup>The initial simulation box size was set at 12.5 nm × 12.5 nm × 12.5 nm.

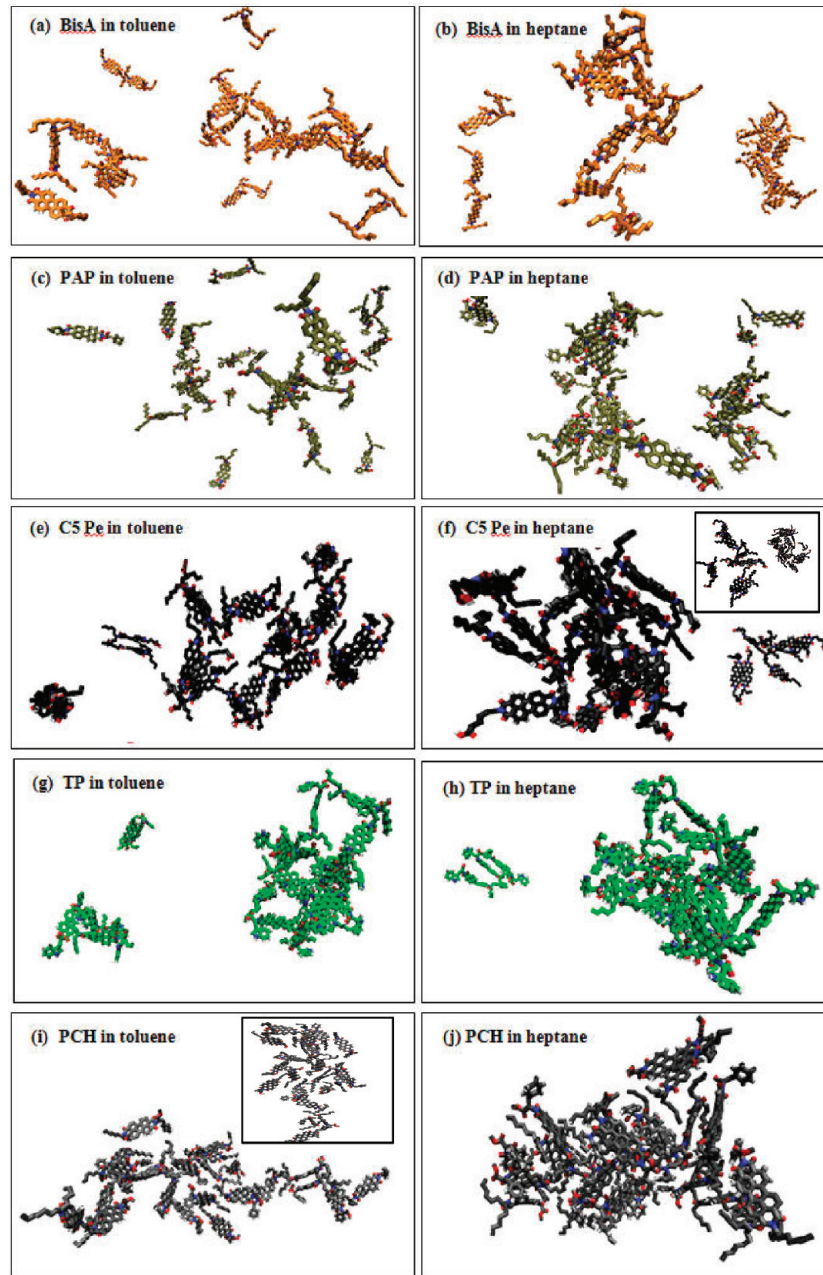


**Figure 1.** Snapshots of molecular configurations of the five PA surfactant molecules in heptane and toluene, taken at the end of 20 ns simulation time. PAP and BisA compounds show a weak aggregate in both solvents. Each molecule is presented by a different color to distinguish one from the other: BisA in orange, PAP in tan, C5 Pe in black, TP in green, and PCH in gray. In all structures oxygen, nitrogen, and hydrogen atoms are presented by red, blue, and white, respectively. All the snapshots are along the z-direction (2-D side view). Top view snapshots of PCH in toluene (i) and C5 Pe in heptane (f) are shown as insets.

were sealed immediately. After filtration, the solutions were thermostatted at 25 °C overnight without disturbance before measurement.

**3.2. Dynamic Light Scattering.** DLS measurements were carried out at a scattering angle of 90° using an ALV 5022 laser light-scattering (LLS) instrument equipped with a cylindrical He–Ne laser (model 1145p-3083; output power = 22 mW at  $\lambda$  = 632.8 nm) in combination with an ALV SP-86 digital correlator of a sampling time range from 25 ns to 40 ms. The LLS cell was held in an index matching vat filled with high-purity, dust-free toluene. The temperature of the experiments was controlled within  $\pm 0.02$  °C by a thermostat. The DLS experiments were completed in 10 min and repeated at least

twice. The CONTIN program supplied with the correlator was used to calculate  $G(D)$  and  $R_h$  (Supporting Information).

## 4. RESULTS AND DISCUSSION

**4.1. Nanoaggregate Formation and Growth.** Figure 1 shows snapshots of the simulation box at  $t = 20$  ns for each of the PA surfactant molecules in the two solvents. From these snapshots we can directly observe that all PA surfactant molecules form nanoaggregates to varying degrees of association. For example, BisA and PAP show smaller, less structured aggregates while C5 Pe and TP form larger aggregates in both solvents. Furthermore, BisA and PAP in toluene show the least aggregation among all of the simulations

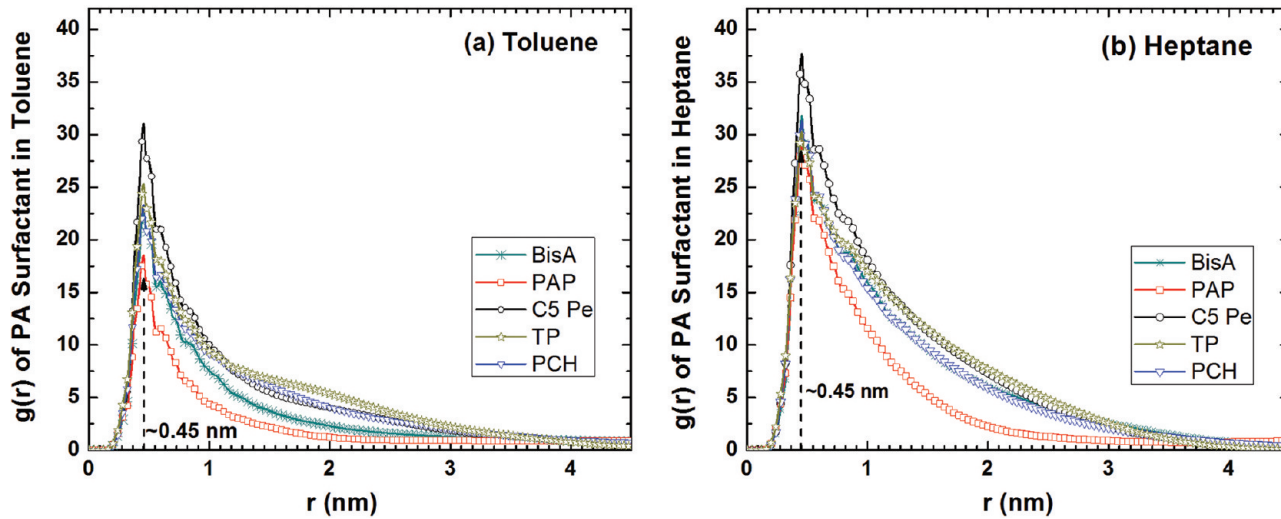


**Figure 2.** Radial distribution functions averaged over the last 2 ns of the simulation time (18–20 ns) of PA surfactant molecules in toluene (a) and heptane (b) at 298 K.

**Table 3. Radius of Gyration, SASA:AV, and Number of Aggregated Molecules in a Large Nanoaggregate Cluster of the Simulated System**

PA surfactant	(SASA/AV) <sub>monomer</sub> (nm <sup>-1</sup> )	(SASA/AV) <sub>nanoaggregate</sub> (nm <sup>-1</sup> )	N <sub>molecules nanoaggregate</sub>	R <sub>g monomer</sub> (nm)	R <sub>g nanoaggregate</sub> (nm)
PA Surfactant Molecules in Toluene					
BisA <sup>a</sup>	6.4 ± 0.10			0.65 ± 0.01	
PAP <sup>a</sup>	6.3 ± 0.13			0.67 ± 0.02	
C5 Pe	6.4 ± 0.10	4.9 ± 0.12	3	0.69 ± 0.01	0.76 ± 0.01
TP	6.3 ± 0.11	4.7 ± 0.01	8	0.68 ± 0.02	1.29 ± 0.20
PCH	6.2 ± 0.09	5.3 ± 0.13	3	0.65 ± 0.02	0.86 ± 0.05
PA Surfactant Molecules in Heptane					
BisA	6.2 ± 0.14	4.9 ± 0.02	4	0.64 ± 0.01	0.96 ± 0.01
PAP	6.3 ± 0.09	4.7 ± 0.10	4	0.67 ± 0.02	0.93 ± 0.01
C5 Pe	6.4 ± 0.09	4.8 ± 0.02	7	0.69 ± 0.02	1.15 ± 0.10
TP	6.3 ± 0.07	4.1 ± 0.01	21	0.67 ± 0.01	2.62 ± 0.23
PCH	6.2 ± 0.05	3.7 ± 0.01	20	0.65 ± 0.01	1.82 ± 0.16

<sup>a</sup>BisA and PAP in toluene does not form nanoaggregate clusters. The R<sub>gx</sub>, R<sub>gy</sub>, and R<sub>gz</sub> of the respective PA surfactant molecules are shown in the Supporting Information, section SI 2. The mean value was obtained over the last 1 ns of the simulation time.

performed in this study. However, loosely packed and fairly large aggregates of C5 Pe and TP are noticeable in both toluene and heptane. Thus, the MD snapshots qualitatively indicate that C5 Pe and TP tend to form aggregates in both solvents, and their tendency to aggregate in heptane is far greater than in toluene.

Previous experimental and computational studies have shown significant aggregation of PA moieties in both heptane and toluene. However, the extent of their aggregation and association in toluene is rather limited, and they terminate at the nanoaggregation level.<sup>10,44,45,61–64</sup> Visual inspection of molecular trajectories reveals that BisA molecules prefer T-stacking or tail-to-tail arrangements with minimum  $\pi$ – $\pi$  stacking due to their strong steric hindrance associated with the branched side chains. In contrast, PAP and PCH show a much different aggregation behavior despite their similar structural features.

Figure 2 shows the radial distribution functions (RDFs) of PA surfactant molecules away from a reference polyaromatic surfactant molecule,  $g(r)$ . These RDFs are the average over the last 2 ns of the simulations (18–20 ns) for all of the PA surfactant molecules in toluene and heptane. It is interesting to note the similar peak positions and shapes of the RDFs among

these PA surfactant compounds in both toluene and heptane. In both solvents three peaks are seen at the regions of 0.45, 0.60, and 0.82 nm. Interestingly, irrespective of the nature of the solvent, the positions of these three peaks remain almost identical for all of the PA surfactant molecules. Similar observation was noticed in our previous work on putative model compounds in toluene and heptane.<sup>44,45</sup> In heptane, these PA surfactant molecules tend to show a slightly broader peak, mainly due to extended nanoaggregate formation and growth. In contrast, a relatively sharper peak of the  $g(r)$  in toluene indicates the formation of more structured nanoaggregates in toluene than in heptane.

To investigate the role of different functional groups in the nanoaggregate formation and growth, we monitored the radial distribution peak heights of PA surfactant molecules as a function of time in both solvents (see Supporting Information, section SI 1). A close examination of the time evolution of the pair correlation function reveals that the nanoaggregates were fully developed and become stable over a shorter simulation time (less than 6 ns) in toluene than in heptane. In heptane, the growth of larger aggregates was visible even beyond 10 ns. Interestingly, although C5 Pe, TP, and PAP molecules all have a polar -COOH functional group in their side chains, the

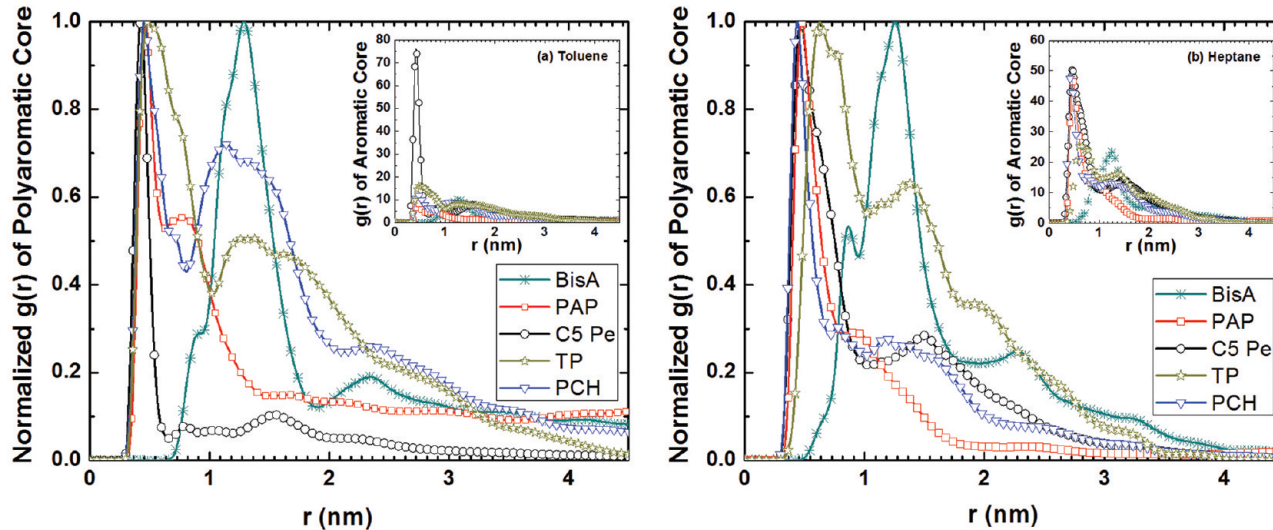


**Figure 3.** Normalized radial distribution functions,  $g(r)/g(r)_{\text{max peak}}$ , of polyaromatic core (perylene core) averaged over the last 2 ns of the simulation time (18–20 ns) in toluene (a) and heptane (b) at 298 K. BisA does not form polyaromatic  $\pi-\pi$  stacking due to its strong steric hindrance in both solvents (inset).

tendency for these molecules to aggregate in both solvents varies significantly. TP has a high tendency to aggregate in both solvents. PAP, on the other hand, shows a weak tendency to aggregate in toluene.

To determine more specifically the impact of -COOH functional group on nanoaggregation, PCH and PAP molecules were closely studied in this work. Results indicate that these molecules in toluene exhibit little differences in the aggregate formation and growth. PAP shows a lower peak height in toluene. Here, the change from -COOH to -COOCH<sub>3</sub> functionality enhances nanoaggregate formation and growth in toluene. In heptane, both compounds show similar peak heights. The observed disparity in toluene is attributed to the polarity difference of the molecules and their effect on hydrogen bonding. It is known that -COOCH<sub>3</sub> is less polar with limited opportunity for hydrogen bonding than -COOH. Therefore, the polarity and hydrogen bonding formation of the side chains in toluene contribute to some extent to altering the nanoaggregate formation and growth.

In Table 3 we report the radius of gyration ( $R_g$ ) and the variation of the ratio between the solvent-accessible surface area (SASA) and the accessible volume (AV), and the number of molecules ( $N$ ) in a large nanoaggregate cluster and the free PA surfactant molecule in the simulation system. The criterion for determining the number of associated molecules per nanoaggregate is by the *linkage algorithm* with a cutoff distance of 0.5 nm, which is within the range of  $\pi-\pi$  stacking.<sup>39–41,65,66</sup> In both toluene and heptane, the single surfactant molecules for all PA surfactants were found to have similar radius of gyration and SASA:AV. However, these PA surfactants form nanoaggregates of different structures. This finding suggests that the concept of critical molecular packing parameter widely accepted for predicting the geometry of molecular aggregates in aqueous solutions is inapplicable to predicting molecular aggregation of the PA surfactants in an organic solvent.

The number of molecules, radius of gyration, and SASA:AV of the large nanoaggregate cluster of the PA surfactant molecules show a significant variation from one another in both heptane and toluene. The nanoaggregates of C5 Pe, for example, show a larger SASA:AV but a smaller  $N$  than the

nanoaggregates formed from TP molecules in heptane. This higher SASA:AV indicates that C5 Pe molecules in heptane exhibit less compact, rodlike nanoaggregate structures while TP compounds form nanoaggregates relatively compact and spherical in shape. In toluene, on the other hand, PCH and TP compounds show the highest and lowest SASA:AV, respectively. The radius of gyration values in  $x$ ,  $y$ , and  $z$  directions were used to determine qualitatively the shape of the large nanoaggregate cluster.

#### 4.2. $\pi-\pi$ Stacking with Side Chain Terminal Groups.

Considering the complex nature of the interactions in PA surfactant molecules, it would be valuable to study the effect of side chains in PA surfactant on  $\pi-\pi$  stacking and hence nanoaggregation of these types of surfactants. The presence of side chains is anticipated to hinder the  $\pi-\pi$  stacking and hydrogen-bonding by steric hindrance, retarding molecular aggregation. To study such effect, RDF between the center six-membered rings of the polyaromatic cores (perylene core) was calculated. Figure 3 shows the RDF normalized with respect to the first peak height, with the actual  $g(r)$  being shown in the insets. Among all of the RDFs, only C5 Pe in toluene shows a remarkably sharp first peak at around 0.45 nm, indicating a strong dimerization. All remaining simulations show variable structures of molecular association of these PA surfactant molecules in the two solvents, depending on the nature of side chains. The first peak at around 0.45 nm in both solvents corresponds to the formation of strong polyaromatic  $\pi-\pi$  stacking of the PA surfactant molecules. These values are confirmed explicitly by calculating the mean distance among the polyaromatic cores of these molecules as shown in Table 4.

**Table 4.** Mean Distance between Two Polyaromatic Cores

compound	toluene (nm)	heptane (nm)
BisA	negligible stacking	negligible stacking
PAP	$0.3975 \pm 0.0217$	$0.3920 \pm 0.0115$
C5 Pe	$0.3880 \pm 0.0056$	$0.4040 \pm 0.0100$
TP	$0.4110 \pm 0.0085$	$0.4020 \pm 0.0100$
PCH	$0.4150 \pm 0.0038$	$0.3868 \pm 0.0059$

The results in Figure 3 show that the normalized RDF has a strong first peak at around 0.45 nm for all of the compounds except for BisA. The width of the first peak correlates well with the number of stacked monomers present in a nanoaggregate. In toluene, C5 Pe exhibits clearly the formation of stacked dimers, whereas PAP, PCH, and TP show increasingly higher levels of stacking association between the polyaromatic cores. The presence of a second peak in the RDFs at around 1.16 nm (1.1–1.3 nm) indicates the formation of perpendicularly associated (T-shaped) structures. Note that BisA in toluene shows a weakly associating T-shaped stacking configuration at around 1.23 nm. The RDFs in Figure 3b show quite similar  $\pi-\pi$  stacking except that the association of C5 Pe, PAP, and PCH becomes more comparable. These results reveal that BisA with an aliphatic functional group in both side chains does prevent the formation of polyaromatic  $\pi-\pi$  stacking due to its strong steric hindrance in both solvents. For the other PA surfactants, we observed varying degrees of stacking association.

C5 Pe has a high tendency to dimerize in toluene (see the inset of Figure 3a), but these molecules do not form large stacking associations. The preference for dimerization arises from its stronger steric hindrance due to the presence of long and linear alkyl side chains in C5 Pe molecules as compared to PAP, TP, and PCH. For PAP, TP, and PCH in toluene, the aromatic or heteroaromatic group, such as benzene or indole as a side chain, tends to have lower steric hindrance to the formation of larger associated structures. This lower steric hindrance associated with these molecules in toluene results from the strong interactions between the toluene solvent molecules and the aromatic side chains. In heptane, all of the PA surfactants studied except for TP and BisA show similar stacking distributions. TP, a nitrogen bearing compound, in heptane also shows a weak polyaromatic  $\pi-\pi$  stacking.

From the RDF obtained from the molecular dynamics simulation, we can conclude that the strong polyaromatic  $\pi-\pi$  stacking is the main driving force for molecular aggregation of PA surfactant in the bulk solutions, which is greatly influenced by the steric hindrance and polarity of its side chains. The more steric barriers the compound possesses, the less likely they stack, in particular, in the presence of aliphatic or alkyl side chains in its good solvent environment. The stacking arrangements of the PA surfactant molecules in heptane are depicted in Figure 4. Similar stacking behavior in toluene was also observed.

**4.3. Radial Distribution Function of Solvent Molecules near Polyaromatic Core.** Figure 5 shows the RDF of solvent molecules around the polyaromatic core of the PA surfactant molecules. The RDF in Figure 5 shows how the solvent molecules associate with the polyaromatic cores. For toluene which readily solubilizes the PA surfactants, there is no significant short-range structure of the solvent molecules. The first peak of the solvent distribution appears beyond 0.5 nm, suggesting that the solvent molecules are excluded from the interstices of the stacked polyaromatic cores (Table 4). Increased levels of dimerization lead to a reduction in solvent accessibility of the polyaromatic cores, which is evident by the reduction in the first peak of the  $g(r)$  curve for C5 Pe in toluene. With increased association between the polyaromatic cores in heptane, the solvent distribution around the polyaromatic rings in Figure 5b shows a much lower  $g(r)$  as compared to toluene but has a more prominent peak.

The solvent accessible surface area (SASA) of the various model PA surfactant molecules in toluene and heptane is

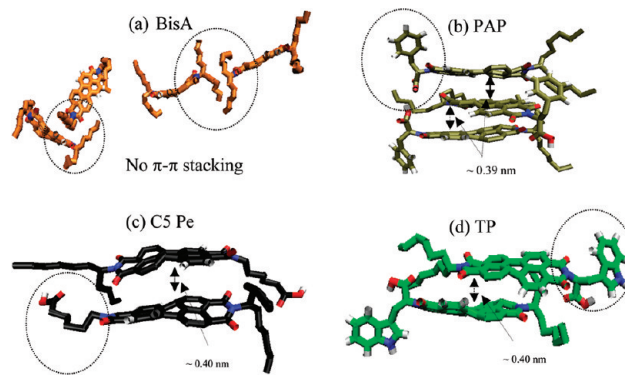


**Figure 4.** Configuration and steric hindrances (dotted circles) of polyaromatic stacking between two PA surfactant molecules: (a) BisA–BisA T-stacking or tail-to-tail stacking, (b) PAP–PAP  $\pi-\pi$  polyaromatic stacking, (c) C5 Pe–C5 Pe  $\pi-\pi$  polyaromatic stacking, and (d) TP–TP  $\pi-\pi$  polyaromatic stacking. The snapshots were taken at the end of 20 ns simulation time. PCH and PAP show similar stacking arrangements, but the extent of their stacking is different.

depicted in Figure 6a,b, respectively. One would expect a systematic decrease in SASA as the molecules associate. The formation of T-stacks or imperfect association structures will not result in a significant decrease in the SASA. However, each  $\pi-\pi$  stack in a dimer will cause a 50% reduction in the SASA. Figure 6a shows how the SASA is related to the degree of association. For BisA and PAP, we see a negligible change in SASA, which correlates well with the lack of aggregation. For TP and C5 Pe, we observe the most significant reduction in SASA. In heptane, the association is more pronounced than in toluene, as shown in Figure 6b.

**4.4. Diffusion of Polyaromatic Surfactants.** To study the impact of side chains of various functional groups on the nanoaggregation dynamics of the PA surfactants, the diffusion coefficient of the PA surfactant molecules was calculated by linear fitting the mean square displacement (MSD) over a fixed time interval of the simulation. From the slope of the mean square displacement, the diffusion coefficient ( $D$ ) of the various PA surfactant molecules was calculated using the Einstein relation:

$$D = \frac{1}{6} \lim_{t \rightarrow \infty} \frac{d}{dt} \langle \overrightarrow{r(t)} - \overrightarrow{r(0)} \rangle^2 \quad (1)$$

where  $\langle \overrightarrow{r(t)} - \overrightarrow{r(0)} \rangle^2$  is the long-time limit of the mean square displacement of the molecules in  $x$ ,  $y$ , and  $z$  directions, taken over all the molecules in the system (see Supporting Information, section SI 3).

To validate the diffusion coefficient obtained from the MSD of the PA surfactant molecules, the diffusion coefficient for a single molecule was also predicted by the Stokes–Einstein equation:

$$D_{SE} = \frac{K_B T}{6\pi\eta(0.678\langle R^2 \rangle^{1/2})} \quad (2)$$

where  $K_B$  is the Boltzmann constant,  $T$  is the absolute temperature,  $\eta$  is the viscosity of the fluid, and  $\langle R^2 \rangle^{1/2}$  is the average radius of gyration over a fixed time interval of the simulation.

The self-diffusivity of heptane and toluene obtained from the slope of the MSD curves is  $(3.42 \pm 0.05) \times 10^{-9}$  and  $(1.88 \pm 0.02) \times 10^{-9} \text{ m}^2 \text{ s}^{-1}$ , respectively. These values agree fairly well

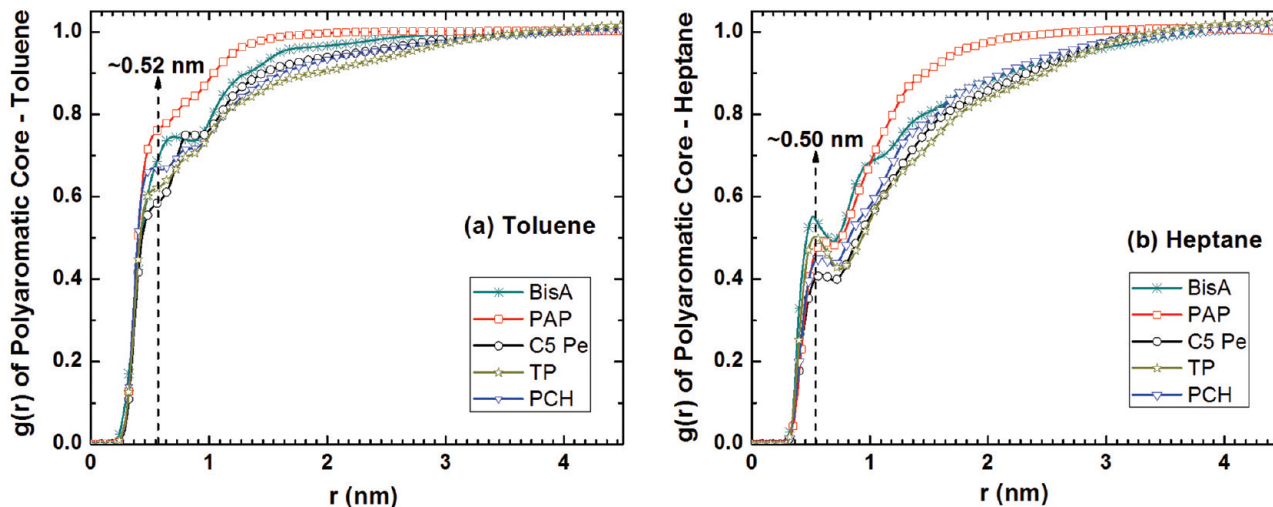


**Figure 5.** RDFs of solvent molecules near a polyaromatic core of the PA surfactant molecules averaged over the last 2 ns of the simulation time (18–20 ns) in toluene (a) and heptane (b) at 298 K.

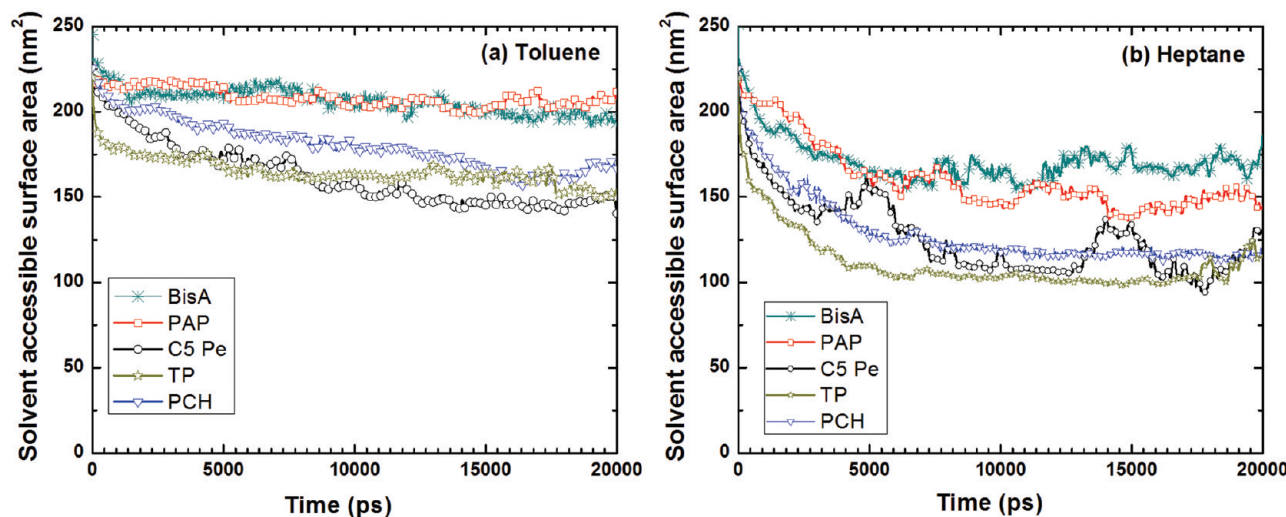


**Figure 6.** Solvent-accessible surface area of the PA surfactant molecules over the simulation time of 20 ns in toluene (a) and heptane (b) at 298 K.

**Table 5. Diffusion Coefficient of PA Surfactant Molecules in Heptane and Toluene**

compound	heptane		toluene	
	$D_{\text{MSD}}$ ( $\times 10^{-9} \text{ m}^2 \text{ s}^{-1}$ )	$D_{\text{Rg}}$ ( $\times 10^{-9} \text{ m}^2 \text{ s}^{-1}$ )	$D_{\text{MSD}}$ ( $\times 10^{-9} \text{ m}^2 \text{ s}^{-1}$ )	$D_{\text{Rg}}$ ( $\times 10^{-9} \text{ m}^2 \text{ s}^{-1}$ )
BisA	$0.232 \pm 0.0002$	$1.31 \pm 0.0140$	$0.172 \pm 0.0001$	$0.846 \pm 0.0120$
PAP	$0.397 \pm 0.0007$	$1.25 \pm 0.0170$	$0.330 \pm 0.0004$	$0.815 \pm 0.0200$
C5 Pe	$0.370 \pm 0.0001$	$1.21 \pm 0.0190$	$0.123 \pm 0.0001$	$0.798 \pm 0.0190$
TP	$0.141 \pm 0.0003$	$1.24 \pm 0.0090$	$0.147 \pm 0.0002$	$0.809 \pm 0.0190$
PCH	$0.164 \pm 0.0004$	$1.29 \pm 0.0120$	$0.167 \pm 0.0001$	$0.841 \pm 0.0150$

with the published experimental values of  $3.12 \times 10^{-9}$  and  $2.26 \times 10^{-9} \text{ m}^2 \text{ s}^{-1}$  for heptane<sup>67</sup> and toluene,<sup>68</sup> respectively. The diffusion coefficient of the PA surfactant molecules in heptane and toluene obtained from eqs 1 and 2 is given in Table 5. The results in Table 5 show that the diffusion coefficient values in both solvents obtained from MSD and the Stokes–Einstein equation are different, indicating strong intermolecular interactions between the PA surfactant molecules, especially above the critical nanoaggregation concentration. The diffusion coefficient obtained from the MSD represents the diffusion coefficient of the aggregates and hence depends on the extent of intermolecular interactions. PAP, for example, shows a

higher diffusion coefficient as compared to the other four PA surfactants in both solvents due to its weak intermolecular interactions.

The direct comparison of the calculated diffusion coefficients from the SE method of the PA surfactant molecules in heptane and toluene reveals that the PA surfactant molecules show a lower diffusivity in toluene than in heptane. In both solvents, the diffusion coefficients of the PA surfactant molecules calculated from the SE method follows the order of BisA > PCH > PAP > TP > C5 Pe, as shown in Table 5. However, the difference in diffusivity of each PA surfactant in these two solvents is insignificant. These findings indicate that the change

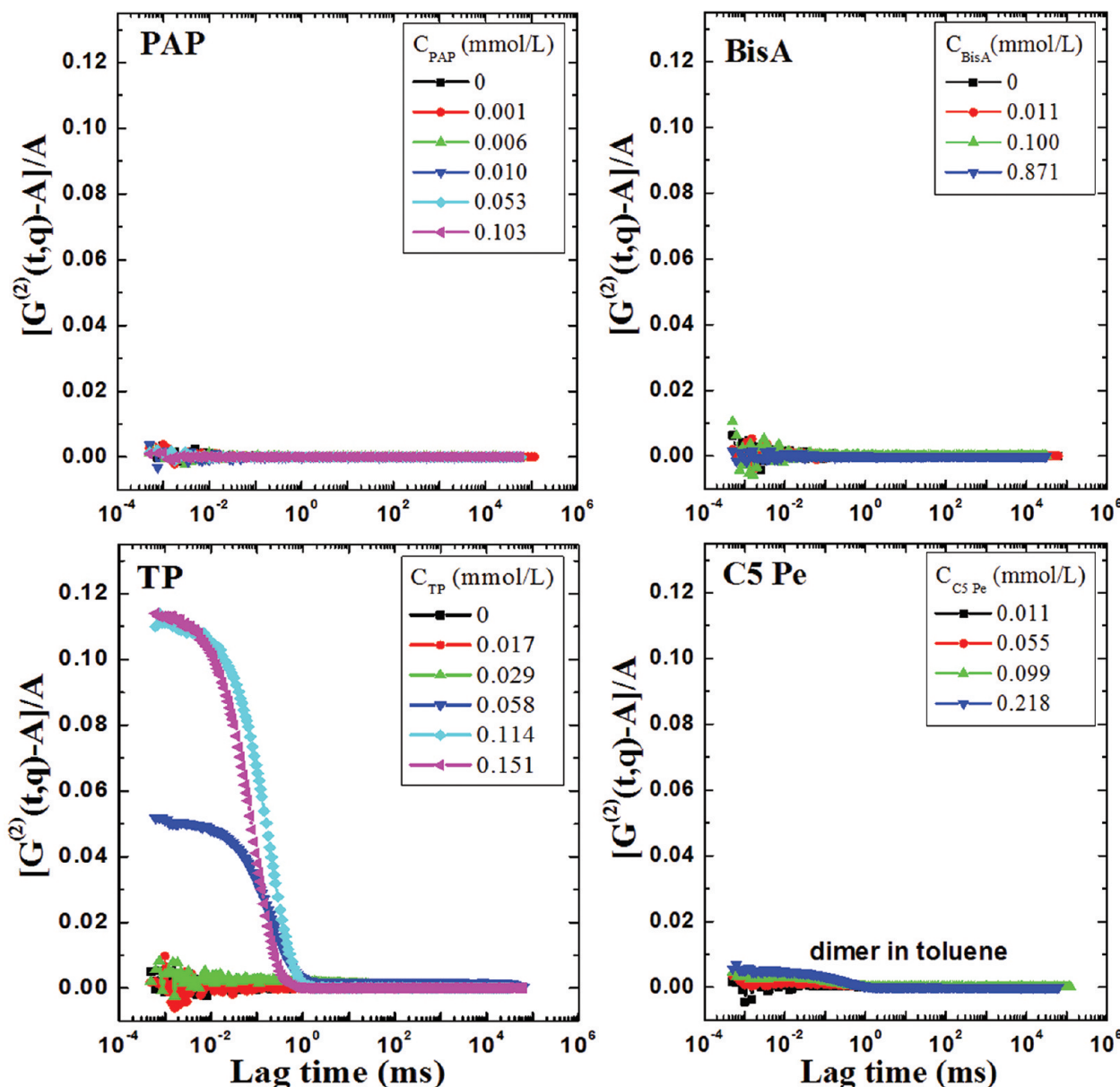


**Figure 7.** Intensity–intensity time correlation as a function of PA surfactant concentration in toluene. BisA and PAP show negligible molecular aggregation at both high and low concentrations, while TP shows strong aggregation at high concentrations. C5 Pe shows dimerization in toluene at all concentrations.

in the molecular structure of the PA surfactant molecules at the side chain does not have a profound impact on the self-diffusivity of the molecules, as anticipated.

**4.5. Aggregation Behavior of PA Surfactant Molecules in Toluene Studied by Dynamic Light Scattering.** Figure 7 shows the dynamic light scattering results of the PA surfactant molecules at different concentrations. Careful inspection of the scattering profiles revealed a negligible decay in the correlation function for PAP and BisA, indicating a negligible aggregation of PAP and BisA in toluene. On the other hand, TP shows two distinct features, depending on the concentration of TP in toluene. At low concentration, no decay is observed, which indicates most of the compounds being dissolved as individual molecules. The correlation function starts to decay at higher concentration, which suggests the aggregation of TP molecules at a higher concentration. These findings are consistent with the MD simulation results

described in section 3.1. Our MD simulation result reveals that PAP and BisA in toluene do not form aggregates due to steric hindrance, while TP is anticipated to form aggregates by increasingly higher levels of stacking between the polyaromatic cores with increasing its concentration. C5 Pe, on the other hand, could form molecular aggregates from the stacked dimers.

It is worthy to mention that the normalized hydrodynamic radius distribution of TP and C5 Pe exhibits a large peak at ~160–230 nm for TP and ~200 nm for C5 Pe if the solution is not filtered by 0.45 μm PTFE filters prior to dynamics light scattering measurement. These results suggest that both molecules form larger aggregates or clusters in toluene. After filtration of the samples using 0.45 μm PTFE filter, only in toluene solution of TP is there still a large peak at ~80 nm; there is no peak in the normalized hydrodynamic radius distribution for C5 Pe in toluene solution (see Supporting

Information, section SI 4). These results suggest that, unlike TP, C5 Pe prefers dimerization in toluene. Unfortunately, since the MD simulation was conducted using a box dimension of 12 nm × 12 nm × 12 nm with the periodic boundary condition and was performed only for 20 ns, it prevented us from observing the much larger aggregates as observed in the DLS measurement.

The scattering intensities of the PA surfactant molecules in toluene can be effectively used to qualitatively indicate the aggregation state of the system. As shown in Figure 8, the

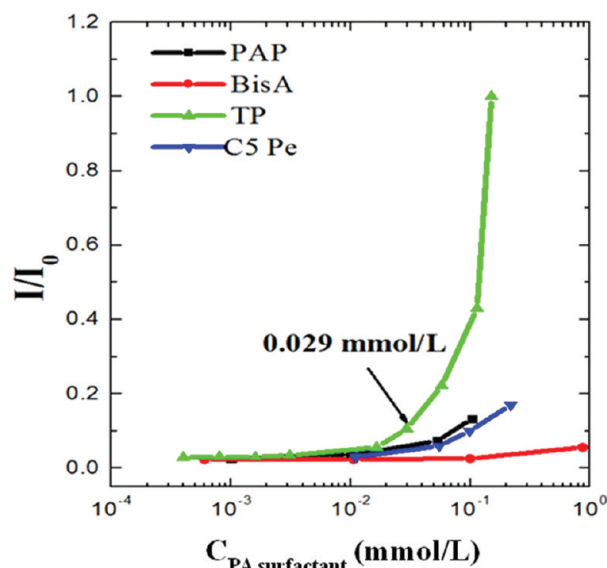


Figure 8. Normalized scattering intensities as a function of PA surfactant concentration in toluene. BisA, PAP and C5 Pe show very low scattering intensities while TP at high concentration shows strong aggregation.

scattering intensities of both PAP and BisA are very low at all the concentrations investigated, indicating that PAP and BisA exist as single molecules in toluene. A sharp upturn of the scattering intensity beyond 0.029 mmol/L reflects the strong aggregation of TP in toluene. The high level of TP molecular aggregation observed in the DLS experiment is consistent with our MD results. Unlike PAP and BisA, TP forms larger aggregates while C5 Pe prefers to form dimers in toluene.

## 5. CONCLUSIONS

The molecular association and nanoaggregate formation dynamics of five polyaromatic surfactants in heptane and toluene were studied using molecular dynamics simulation and dynamic light scattering. Analysis of RDFs and scattering profiles of the PA surfactants show that a change in molecular structure and the polarity of a substituent side chain functional group has a significant impact on molecular association, nanoaggregation dynamics, nanoaggregate structure, and stability of nanoaggregates in both heptane and toluene.

The aggregates of PA surfactant molecules grow to much larger sizes in heptane than in toluene. In toluene, the substitution of tryptophan side chain in TP by phenylalanine in PAP makes PAP to dissolve as individual molecules.

The presence of a branched *n*-alkane side chain in BisA leads to the lowest aggregation and hence the highest SASA:AV of BisA in heptane. In contrast, the presence of a nitrogen-bearing aromatic side chain in TP makes TP to aggregate strongly in

heptane, leading to the lowest SASA:AV due to its less compatible nature with heptane.

Only C5 Pe in toluene exhibits a very sharp first peak at around 0.45 nm in the normalized RDFs of the polyaromatic cores, indicating a strong dimerization. All other PA surfactant molecules show variable structures of molecular association in both toluene and heptane, depending on the nature of the side chains attached to the polyaromatic core. The peaks in the RDF at around 0.45 and 1.23 nm in both solvents correspond to the formation of polyaromatic  $\pi$ – $\pi$  stacking and perpendicular (T-shape) stacking of the PA surfactant molecules, respectively. In the extreme case, BisA with an aliphatic functional group in both side chains does not form polyaromatic  $\pi$ – $\pi$  stacking in both solvents due to its strong steric hindrance. The RDFs of the solvent molecules near the polyaromatic core, on the other hand, show that the solvent molecules are excluded from the interstices of the stacked polyaromatic cores in nanoaggregates.

The PA surfactant molecules in heptane exhibit a higher self-diffusivity than in toluene. However, the change in molecular structure of substituent side chains in the PA surfactants has a negligible impact on their self-diffusivity but a profound impact on their intermolecular interactions, leading to different aggregate diffusion coefficients. The aggregates of PAP, for example, show a higher diffusion coefficient than the aggregates formed from the other four PA surfactants in both solvents due to its weak intermolecular interactions.

In both toluene and heptane, the single (nonaggregated) surfactant molecules for all PA surfactants were found to have similar radius of gyration and SASA:AV, while these PA surfactants form nanoaggregates of a wide range of structures. This finding suggests that the concept of critical molecular packing parameter widely accepted for predicting the geometry of molecular aggregates in aqueous solutions is inapplicable to predicting molecular aggregation of the PA surfactants in an organic solvent.

## ■ ASSOCIATED CONTENT

### § Supporting Information

Tables listing the radius of gyration, the solvent accessible surface area, and the accessible volume of the large nanoaggregate cluster and the free PA surfactant molecule and the radial distribution function and diffusion coefficients of the PA surfactant molecules as a function of time in both solvents, figures showing PA–PA surfactant radial distribution peak heights, the time evolution of PA surfactants, mean square displacement vs time for PA surfactants in organic solvents, the correlation function before filtration, and hydrodynamic radial distributions, and text describing dynamic light scattering. This material is available free of charge via the Internet at <http://pubs.acs.org>.

## ■ AUTHOR INFORMATION

### Corresponding Author

\*E-mail: subir.b@ualberta.ca (S.B.); Zhenghe@ualberta.ca (Z.X.).

### Notes

The authors declare no competing financial interest.

## ■ ACKNOWLEDGMENTS

The authors gratefully acknowledge financial support from the Canada Research Chairs (CRC) program and the NSERC-Industry Research Chair in Oil Sands Engineering. We are also

grateful for the Oil Sands and Coal Interfacial Engineering Facility (OSCIEF)—Energy Innovations for assistance and computational resources. Financial support through the Petromaks program (Norwegian Research Council) and JIP 1 (Ugelstad Laboratory) is gratefully acknowledged.

## ■ REFERENCES

- (1) Tao, A. R.; Habas, S.; Yang, P. *Small* **2008**, *4*, 310–325.
- (2) Hvidsten, T. R.; Lægreid, A.; Kryshtafovych, A.; Andersson, G.; Fidelis, K.; Komorowski, J. *PLoS One* **2009**, *4*, No. e6266.
- (3) Song, K. B.; Damodaran, S. *J. Agric. Food Chem.* **1987**, *35*, 236–241.
- (4) Klebe, G. *J. Mol. Med.* **2000**, *78*, 269–281.
- (5) Kim, H. S.; Hartgerink, J. D.; Ghadiri, M. R. *J. Am. Chem. Soc.* **1998**, *120*, 4417–4424.
- (6) Ryu, J. H.; Hong, D. J.; Lee, M. *Chem. Commun. (Cambridge, U.K.)* **2008**, *9*, 1043–1054.
- (7) Hoeben, F. J. M.; Jonkheijm, P.; Meijer, E. W.; Schenning, A. P. H. *J. Chem. Rev.* **2005**, *105*, 1491–1546.
- (8) Müllen, K.; Jürgen, P. *R. Acc. Chem. Res.* **2008**, *4*, 511–520.
- (9) Schenning, A. P. H. J.; Jonkheijm, P.; Hoeben, F. J. M.; van Herrikhuyzen, J.; Meskers, S. C. J.; Meijer, E. W.; Herz, L. M.; Daniel, C.; Silva, C.; Phillips, R. T.; Friend, R. H.; Beljon, D.; Miura, A.; De Feyter, S.; Zdanowska, M.; Uji-i, H.; De Schryvere, Chen, Z.; Würthner, F.; Mas-Torrent, M.; den Boer, D.; Durkut, M.; Hadley, P. *Synth. Met.* **2004**, *147*, 43–48.
- (10) Boek, E. S.; Yakovlev, D. S.; Headen, T. F. *Energy Fuels* **2009**, *23*, 1209–1219.
- (11) Oh, K.; Ring, T. A.; Deo, M. D. *J. Colloid Interface Sci.* **2008**, *271*, 212–219.
- (12) Mackie, I. D.; DiLabio, G. A. *J. Phys. Chem.* **2008**, *112*, 10968–10976.
- (13) Avlasevich, Y.; Li, C.; Müllen, K. *J. Mater. Chem.* **2010**, *20*, 3814–3826.
- (14) Fischer, M. K. R.; Kaiser, T. E.; Würthner, F.; Bäuerle, P. *J. Mater. Chem.* **2009**, *19*, 1129–1141.
- (15) Reghu, R. R.; Bisoyi, H. K.; Grazulevicius, J. V.; Anjukandi, P.; Gaidelis, V.; Jankauskas, V. *J. Mater. Chem.* **2011**, *21*, 7811–7819.
- (16) Ilhan, F.; Tyson, D. S.; Stasko, D. J.; Kirschbaum, K.; Meador, M. A. *J. Am. Chem. Soc.* **2006**, *128*, 702–703.
- (17) Facchetti, A. *Chem. Mater.* **2011**, *23*, 733–758.
- (18) Huang, Y.; Quan, B.; Wei, Z.; Liu, G.; Sun, L. *J. Phys. Chem.* **2009**, *113*, 3929–3933.
- (19) Li, C.; Liu, M.; Pschirer, N. G.; Baumgarten, M.; Müllen, K. *Chem. Rev.* **2010**, *110*, 6817–6855.
- (20) Hippius, C.; Schlosser, F.; Vysotsky, O. M.; Böhmer, V.; Würthner, F. *J. Am. Chem. Soc.* **2006**, *128*, 3870–3871.
- (21) Mizoshita, N.; Tani, T.; Inagaki, S. *Adv. Funct. Mater.* **2011**, *21*, 3291–3296.
- (22) Law, K.-Y. *Chem. Rev.* **1993**, *93*, 449–486.
- (23) Diaz-Garcia, M. A.; Calzado, E. M.; Villalvilla, J. M.; Boj, P. G.; Quintana, J. A.; Céspedes-Guirao, F. J.; Fernández-Lázaro, F.; Sastre-Santos, A. *Synth. Met.* **2009**, *159*, 2293–2295.
- (24) Choi, H.; Paek, S.; Song, J.; Kim, C.; Cho, N.; Ko, J. *Chem. Commun. (Cambridge, U.K.)* **2011**, *47*, 5509–5511.
- (25) Würthner, F.; Sautter, A. *Chem. Commun. (Cambridge, U.K.)* **2000**, 445–446.
- (26) Lee, M.; Cho, B.; Jang, Y.; Zin, W. *J. Am. Chem. Soc.* **2000**, *122*, 7449–7455.
- (27) Rybtchinski, B. *ACS Nano* **2011**, *9*, 6791–6818.
- (28) Zhang, X.; Rehm, S.; Safont-Sempere, M.; Würthner, F. *Nature Chem.* **2009**, *1*, 623–629.
- (29) Baram, J.; Shirman, E.; Ben-Shitrit, N.; Ustinov, A.; Weissman, H.; Pinkas, I.; Wolf, S. G.; Rybtchinski, B. *J. Am. Chem. Soc.* **2008**, *130*, 14966–14967.
- (30) Wang, K.; Guo, D.; Jiang, B.; Sun, Z.; Liu, Y. *J. Phys. Chem.* **2010**, *114*, 101–106.
- (31) Zhang, X.; Chen, Z.; Würthner, F. *J. Am. Chem. Soc.* **2007**, *129*, 4886–4887.
- (32) Marshall, G. A.; Rodgers, P. R. *Acc. Chem. Res.* **2004**, *37*, 53–59.
- (33) Speight, J. G.; Long, R. B. *Pet. Sci. Technol.* **1996**, *14*, 1–12.
- (34) Speight, J. G. *Oil Gas Sci. Technol.* **2004**, *59*, 467–477.
- (35) Rogel, E. *Colloids Surf., A* **1995**, *104*, 85–93.
- (36) Pierre, C.; Barré, L.; Pina, A.; Moan, M. *Oil Gas Sci. Technol.* **2004**, *59*, 489–501.
- (37) Spiecker, P. M.; Gawrys, K. L.; Trail, C. B.; Kilpatrick, P. K. *Colloids Surf., A* **2003**, *220*, 9–27.
- (38) Nordgård, L. E.; Sjöblom, J. *J. Dispersion Sci. Technol.* **2008**, *29*, 1114–1122.
- (39) van der Spoel, D.; Lindahl, E.; Hess, B.; Groenhof, G.; Mark, A. E.; Berendsen, H. J. C. *J. Comput. Chem.* **2005**, *26*, 1701–1718.
- (40) Berendsen, H.; van der Spoel, D.; Drunen, V. R. *GROMACS: A message-passing parallel molecular dynamics implementation.* *Comput. Phys. Commun.* **1995**, *91*, 43–56.
- (41) Lindahl, E.; Hess, B.; van der Spoel, D. *J. Mol. Mod.* **2001**, *7*, 306–317.
- (42) Oostenbrink, C.; Villa, A.; Mark, A.; van Gunsteren, W. *J. Comput. Chem.* **2004**, *25*, 1656–1676.
- (43) Oostenbrink, C.; Soares, T. A.; van der Vegt, N. F. A.; van Gunsteren, W. F. *Eur. Biophys. J.* **2005**, *34*, 273–284.
- (44) Kuznicki, T.; Masliyah, J. H.; Bhattacharjee, S. *Energy Fuels* **2008**, *22*, 2379–2389.
- (45) Kuznicki, T.; Masliyah, J. H.; Bhattacharjee, S. *Energy Fuels* **2009**, *23*, 5027–5035.
- (46) Nordgård, L. E.; Landsem, E.; Sjöblom, J. *Langmuir* **2008**, *24*, 8742–8751.
- (47) Nordgård, L. E.; Sørland, G.; Sjöblom, J. *Langmuir* **2010**, *26*, 2352–2360.
- (48) *Chem3D Ultra 10.0*; Cambridge Scientific Software: Cambridge, MA, USA, 2006.
- (49) Schuettelkopf, A. W.; van Aalten, D. M. F. *Acta Crystallogr.* **2004**, *D60*, 1355–1363.
- (50) Berendsen, C. J. H.; Postma, M. P. J.; DiNola, A.; Haak, R. J. *J. Chem. Phys.* **1984**, *81*, 3684–3690.
- (51) Nosé, S. *Mol. Phys.* **1984**, *52*, 255–268.
- (52) Hoover, W. G. *Phys. Rev. A* **1985**, *31*, 1695–1697.
- (53) Parrinello, M.; Rahman, A. *J. Appl. Phys.* **1981**, *51*, 7182–7190.
- (54) *Knovel Critical Tables*, 2nd ed.; Knovel: New York, NY, USA, 2008; available online at [http://www.knovel.com/web/portal/browse/display?\\_EXT\\_KNOVEL\\_DISPLAY\\_bookid=761&VerticalID=0](http://www.knovel.com/web/portal/browse/display?_EXT_KNOVEL_DISPLAY_bookid=761&VerticalID=0) (accessed on 20 May 2011).
- (55) van der Spoel, D.; van Buuren, A. R.; Apol, E.; Meulenhoff, P. J.; Tielemans, D. P.; Sijbers, A.; Feenstra, K. *The GROMACS Manual* (Version 3.3); Groningen University: Groningen, The Netherlands, 2004.
- (56) Verlet, L. *Phys. Rev.* **1967**, *159*, 98–103.
- (57) Hockney, R. W. The potential calculation and some applications. In *Methods of Computational Physics*; Alder, B., Frenck, S., Rotenberg, M., Eds.; Academic Press: New York, NY, USA, 1970; pp 135–211.
- (58) Essman, U.; Perera, L.; Berkowitz, L. M.; Darden, T.; Le, H.; Pedersen, G. *J. Chem. Phys.* **1995**, *103*, 8577–8592.
- (59) Hess, B.; Bekker, H.; Berendsen, C. J. H.; Fraaije, M. E. G. J. *J. Comput. Chem.* **1997**, *18*, 1463–1472.
- (60) Humphrey, W.; Dalke, A.; Schulten, K. *J. Mol. Graphics* **1996**, *14*, 33–38.
- (61) Andreatta, G.; Goncalves, C. C.; Buffin, G.; Bostrom, N.; Quintella, C. M.; Arteaga-Larios, F.; Perez, E.; Mullins, C. O. *Energy Fuels* **2005**, *19*, 1282–1289.
- (62) Headen, T. F.; Boek, E. S.; Skipper, N. T. *Energy Fuels* **2009**, *23*, 1220–1229.
- (63) Andreatta, G.; Bostrom, N.; Mullins, O. C. *Langmuir* **2005**, *21*, 2728–2736.
- (64) Goncalves, S.; Castillo, J.; Fernández, A.; Hung, J. *Fuel* **2004**, *83*, 1823–1828.

- (65) Shao, J.; Tanner, S. W.; Thompson, N.; Cheatham, E. T. *J. Chem. Theory Comput.* **2007**, *3*, 2312–2334.
- (66) Visheveshwara, S.; Kannan, N. *Protein Eng.* **2000**, *13*, 753–761.
- (67) Douglass, C. D.; McCall, W. D. *J. Phys. Chem.* **1958**, *62*, 1102–1107.
- (68) Antalek, B.; Williams, J. A.; Texter, J. *Phys. Rev. E* **1996**, *54*, 5913–5916.